ChemPhotoChem

Research Article
doi.org/10.1002/cptc.202300091

Chemistry Europe
European Chemical Societies Publishing

www.chemphotochem.org

Special Collection

A BODIPY-Based Molecular Rotor in Giant Unilamellar Vesicles: A Case Study by Polarization-Resolved Time-Resolved Emission and Transient Absorption Spectroscopy

Keshav Kumar Jha,[a, b] Amrutha Prabhakaran,[c] Lukas Spantzel,[d] Rengel Cane Sia,[e] Iván Pérez,[d] Ruben Arturo Arellano-Reyes,[c] Anna Elmanova,[a, b] Anindita Dasgupta,[f, g] Christian Eggeling,[f, g, h] Michael Börsch,[d] Julien Guthmuller,[e] Martin Presselt,[a, b] Tia E. Keyes,[c] and Benjamin Dietzek-Ivanšić*[a, b]

BODIPY and BODIPY-derived systems are widely applied as fluorophores and as probes for viscosity detection in solvents and biological media. Their orientational and rotational dynamics in biological media are thus of vital mechanistic importance and extensively investigated. In this contribution, polarization-resolved confocal microscopy is used to determine the orientation of an amphiphilic BODIPY-cholesterol derivative in homogeneous giant unilamellar vesicles (GUV) made from 1,2-dioleoyl-sn-glycero-3-phosphocholine (DOPC). The BODIPY-moiety of the molecule is placed near the polar headgroups, and the cholesterol moiety is embedded in the membrane along the acyl chain of the lipids. The rotational relaxation of fluorophore is conventionally investigated by time-resolved emission anisotropy (TEA); and this method is also used here. However, TEA depends on the emission of the fluorophore and may not be useful to probe rotational dynamics of the non-emissive triplet states. Thus, we employ femtosecond transient absorption anisotropy (TAA), that relies on the absorption of the molecule to complement the studies of the amphiphilic BODIPY in DCM and GUV. The photoinduced anisotropy of the BODIPY molecule in DCM decays tri-exponentially, the decay components (sub-5 ps, 43 ps and 440 ps) of anisotropy are associated with the non-spherical shape of the BODIPY molecule. However, the anisotropy decay in homogenous GUVs follows a biexponential decay; which arises from the wobbling-in-a-cone motion of the non-spherical molecule in the high viscous lipid bilayer media. The observations for the BODIPY-chol molecule in the GUV environment by TAA will extend to the investigation of non-emissive molecules in cellular environment since GUV structure and size resembles the membrane of a biological cell.

[a] K. K. Jha, A. Elmanova, Dr. M. Presselt, Prof. Dr. B. Dietzek-Ivanšić
Leibniz Institute of Photonic Technology Jena
Research Department Functional Interfaces
Albert-Einstein-Straße 9, 07745 Jena (Germany)
E-mail: benjamin.dietzek@leibniz-ipht.de

[b] K. K. Jha, A. Elmanova, Dr. M. Presselt, Prof. Dr. B. Dietzek-Ivanšić
Institute of Physical Chemistry and Abbe Center of Photonics
Friedrich Schiller University Jena
Helmholtzweg 4, 07743 Jena (Germany)
E-mail: benjamin.dietzek@uni-jena.de

[c] Dr. A. Prabhakaran, R. A. Arellano-Reyes, Prof. Dr. T. E. Keyes
School of Chemical Sciences
National Centre for Sensor Research
Dublin City University
Dublin 9 (Ireland)

[d] L. Spantzel, I. Pérez, Prof. Dr. M. Börsch
Single-Molecule Microscopy Group and Center of Medical Optics and Photonics
Jena University Hospital
Nonnenplan 2–4, 07743 Jena (Germany)

[e] R. C. Sia, Dr. J. Guthmuller
Institute of Physics and Applied Computer Science
Faculty of Applied Physics and Mathematics
Gdańsk University of Technology
Narutowicza 11/12, 80233 Gdańsk (Poland)

[f] A. Dasgupta, Prof. Dr. C. Eggeling
Leibniz Institute of Photonic Technology Jena
(Member of the Leibniz Centre for Photonics in Infection Research (LPI), Jena, Germany)
Research Department Biophysical Imaging
Albert-Einstein-Straße 9, 07745 Jena (Germany)

[g] A. Dasgupta, Prof. Dr. C. Eggeling
Institute of Applied Optics and Biophysics
Friedrich Schiller University Jena
Helmholtzweg 4, 07743 Jena (Germany)

[h] Prof. Dr. C. Eggeling
Jena Center for Soft Matter
Philosophenweg 7, 07743 Jena (Germany)

Supporting information for this article is available on the WWW under https://doi.org/10.1002/cptc.202300091

Special Collection An invited contribution to a Special Collection on Ultrafast Spectroscopy

Introduction

The tunable optical properties, large extinction coefficients and high fluorescence quantum yields of BODIPY fluorophores[1] constitute the basis for applications such as molecular rotors,[2,3] photochemical singlet oxygen generation[4] and triplet-triplet annihilation upconversion (TTAUC).[5–7] Meso-substitution of the phenyl ring yields BODIPY derivatives, so-called fluorescent molecular rotors (FMRs), render them suitable for viscosity detection.[2,3] The viscosity of a cell membrane, or its fluidity (the reciprocal viscosity) is critically linked to cell physiology influencing cell adhesion, signaling and cell differentiation. It influences drug permeation and changes to membrane composition with disease state also instigates measurable changes in membrane viscosity.[8–10] Membrane viscosity can be conveniently measured using probes such as FMRs.[3] When changing from low to high viscosity, the intensity of the BODIPY FMR fluorescence and fluorescence lifetime increase due to an increasingly hindered intramolecular rotation.[3,11]

Giant unilamellar vesicles (GUVs) are suitable models for cellular membranes.[12] The rotational relaxation time, organization and orientation of various fluorophores (including BODIPYs) in GUVs as well as in cell membranes have been investigated previously.[13–18] A technique routinely used is time-resolved emission anisotropy (TEA).[17-20] However, this approach is restricted to fluorescent molecules with fluorescence decay times exceeding the emission depolarization timescales.[19] In particular in the context of light-driven molecular processes, e.g., in photodynamic therapy but also in triplet-triplet annihilation upconversion[6] for drug release or activation, non-emissive triplet states might play a key function-determining role. Furthermore, even well-established fluorophores might have very unfavorable emission properties in certain environments,[21–23] e.g., many BODIPY-molecules do not fluoresce in aqueous environments.[1,24] In such cases, time-resolved transient absorption anisotropy (TAA) might complement time-resolved fluorescence anisotropy measurements to investigate molecular motion, e.g., in cells, cell membranes or cell membrane models. TAA probes the rotational diffusion of both emissive and non-emissive molecules by using two orthogonally polarized probe beams (see Figure 1 for a schematic depiction).[25–27] For instance, nanosecond transient absorption anisotropy has been used to evaluate rotational diffusion coefficients of bacteriorhodopsin (BR) in dimyristoylphosphatidylcholine (DMPC) and egg phosphatidylcholine.[28] Here, we present – to the best of our knowledge – the first femtosecond transient absorption anisotropy of BODIPY-derivatives in GUVs to investigate the local mobility of the chromophoric part of the molecules (see Figure 1) bound to the model membrane by an extended molecular linker and relate this data to TEA results on the same fluorophore. Complementing the TAA and TEA with polarization-resolved confocal microscopy, the orientation and fluctuation of the BODIPY fluorophores in the lipid bilayer are elucidated.

The BODIPY-Ar-Chol (See Figure 1) molecule presents a paradigm BODIPY-FMR, as it embeds into homogeneous and ternary GUVs and is soluble in a range of solvents, *e.g.*, dichloromethane (DCM), chloroform and acetonitrile (ACN).[1] In particular, the molecule can be used to target mammalian cells, where it permeates the membrane and localizes into lipid droplets.[1] As such the BODIPY-Ar-Chol presents a promising molecular probe to spectroscopically explore molecular properties on a sub-cellular level.[24]

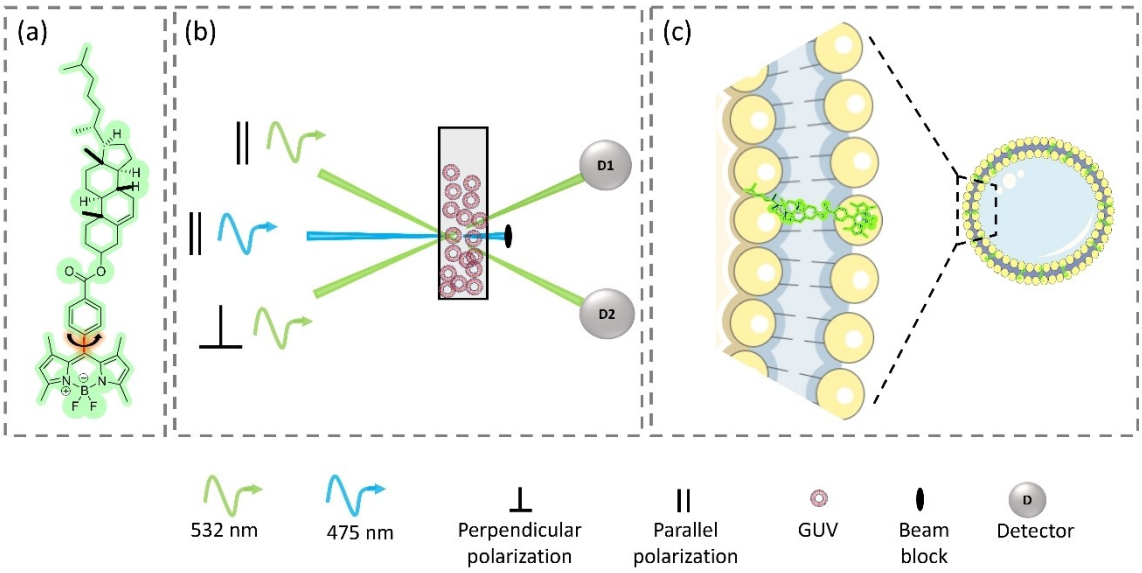

Figure 1. (A) Structure of the BODIPY-Ar-Chol molecule and its intramolecular rotation (shown by an arrow) as a BODIPY-phenyl molecular rotor. (B) Schematic diagram of the transient absorption anisotropy measurement of the BODIPY-Ar-Chol molecules in GUVs. (C) Enlarged GUV model and the BODIPY-Ar-Chol in the lipid bilayer.

Experimental Details

Samples

BODIPY-Ar-chol molecules are synthesized according to the protocol published earlier.[1] GUVs were prepared using a mixture of 1,2-Dioleoyl-sn-glycero-3-phosphocholine (DOPC) lipid of 5 mM and a 15 μM solution of the dye (BODIPY-Ar-Chol) in chloroform. The mixed solution (DOPC and dye) is drop casted (1 μL) on a pair of indium tin oxide (ITO)-coated glass slides and dried in a desiccator under vacuum conditions to completely evaporate the solvent. The dried ITO slides were placed in the Vesicle Prep Pro (Nanion Technologies) and a greased O-ring was put on the conductive side of a slide, which was filled with 230 mM sucrose solution. Another ITO slide was used to seal the sucrose-filled O-ring with a conductive side toward the solution before electroformation. First, the voltage was raised from 0 to 3 V within 5 minutes, then 3 V was maintained for 170 minutes at 10 Hz frequency, followed by a voltage ramp from 3 to 0 V in 5 minutes. Subsequently, the GUVs were collected in an Eppendorf tube. The temperature was maintained at 37 °C during the electroformation process. For time-resolved measurements, the dye was dissolved in chloroform to yield an absorbance of about 0.3 at 470 nm and placed in 1 mm pathlength quartz cuvettes. GUV samples were measured using the same cuvettes.

Steady-State Spectroscopy

Steady-state absorption was measured with a Jasco V780 UV/vis/NIR spectrophotometer. Emission was recorded using an FLS980 emission spectrophotometer (Edinburgh Instruments) utilizing a xenon lamp as an excitation source (ozone-free 450 W). All steady-state measurements were performed using 1 cm pathlength quartz cuvettes.

Transient Emission Spectroscopy

The fluorescence intensity decays were recorded in quartz cuvettes using a modular fluorescence lifetime spectrometer (FluoTime 200, PicoQuant) with time-correlated single photon counting (TCSPC). The light source was a pulsed LED with 459 nm emission, 1 ns pulse width and a repetition rate of 10 MHz. Emission was detected at 515 nm. Glan-Taylor prisms served to select the polarization of the excitation and the emission. The G-factor of the setup was calculated from the fluorescence intensity decay histograms of a solution of Rhodamine 110 yielding a value of $G = 1.34$.

Transient Absorption Spectroscopy and Transient Absorption Anisotropy

Femtosecond time-resolved absorption and transient absorption anisotropy measurements were performed using a home-built experimental setup.[29,30] Briefly, a mode-locked Ti: sapphire laser produced 80 fs pulses centered at 800 nm (repetition rate of 1 kHz), which were split into two beams to pump two optical parametric amplifiers (TOPAS, LightConversion) in order to generate pump and probe pulses at 470 and 525 nm, respectively. The probe beam was split into two probe beams, the polarization of one beam was parallel ($I_{\parallel}$) and of another beam was perpendicular to the pump polarization ($I_{\perp}$), see Figure 1 b. The two probe beams and the pump beam spatially and temporally overlapped on the sample. The transmitted probe beams were detected by photodiodes. The magic angle ($I_{54.7°}$) signal and the transient absorption anisotropy were calculated using the signals recorded at parallel and perpendicular polarizations. The pump power was kept at 8 μW, for the measurements in solution and vesicles. To cross-validate the setup, we measured the transient absorption anisotropy of $[Ru(bpy)_3]^{2+}$ in acetonitrile (see supplementary information Figure S3), which had been reported in the literature.[25]

Methods of microscopy

Fluorescence lifetime and time-resolved anisotropy images were recorded using a confocal STED microscope (ExpertLine, Abberior Instruments, Göttingen, Germany). The BODIPY fluorophore was excited with a linearly polarized pulsed picosecond laser at 488 nm (repetition rate 40 MHz). BODIPY-Ar-Chol constituted GUVs were imaged at room temperature using a 60x water immersion objective UPLSAPO60XW (n.a. 1.2) from Olympus (Shinjuku, Japan). Fluorescence in the spectral range of 500 to 550 nm was separated by a polarizing beam splitter cube and recorded simultaneously by two single photon counting avalanche photodiodes (SPCM-AQRH-14-TR, Excelitas, Mississauga, Canada) using synchronized TCSPC electronics comprising four synchronized SPC-150 N cards with routers (Becker & Hickl, Berlin, Germany). Time binning of 21 ps for a high time resolution of the fluorescence decays was used. Static anisotropy image analysis was achieved by correcting for the differences in detector sensitivity, by subtracting background intensity, by setting a minimum intensity threshold to select the pixels of the GUV membrane, by calculating the local anisotropy value for each pixel and by correcting for the depolarization factor of the microscope optics.

Alternatively, fluorescence images of the GUV samples (Figure S1) were collected using a Leica TSP inverted (DMi8) confocal microscope with a 40x oil immersion objective. A white light laser tunable in range 470–670 nm was used to excite the sample at 503 nm and the emission was collected between 503–570 nm without a polarizer. The images of immobile GUVs were taken after incubating with 0.1 % agarose solution for 10 minutes.

Computational methods

The quantum chemical calculations were performed with the Gaussian 16 program.[31] Density functional theory (DFT) was employed to calculate the geometry of the ground state (S_0), while time-dependent DFT (TDDFT) was used to compute the singlet (S_1) excited state properties, i.e., energy, S_0-S_1 transition dipole moment (TDM) and geometry. The DFT and TDDFT calculations were done with the MN15[32] exchange-correlation (XC) functional in association with the def2-SVP basis set.[33,34] Density functional dispersion corrections were included using the GD3 model[35–37] using the parameter reported in Goerigk et al[36,37] for MN15. The effects of the solvent (dichloromethane, $\varepsilon = 8.93$) were taken into account by the polarizable continuum model[38] (PCM) using the SMD solvation model.[39] The effects of solvent reorganization on the TDM were estimated by comparing non-equilibrium and equilibrium PCM calculations.

The TDM coordinates (X, Y, Z) are calculated with respect to a molecule-fixed Cartesian frame. The frame is defined so that the X axis connects the central carbon atom and the boron atom of the BODIPY core. The Y axis passes through a carbon atom of the central BODIPY ring, i.e., the Y axis defines the long axis of the BODIPY. The Z axis is perpendicular to the XY plane (see SI, Figure S5). All TDMs coordinates are calculated within this Cartesian frame. Therefore, the calculated rotation angles describe a rotation of the TDM within the molecule-fixed frame.

The ellipsoid axes and lengths were calculated using the Minimum Volume Ellipsoid (MVE) method.[40,41] See the Supporting Information computation section for details.

Results and Discussion

Figure 2 depicts steady-state absorption and emission spectra of BODIPY-Ar-Chol in DCM. The electronic transition S_0-S_1 is centered at around 500 nm, while the fluorescence emission peaks at 514 nm. The extinction coefficient at 503 nm ($6.34 \cdot 10^4$ $M^{-1} \cdot cm^{-1}$) and emission maximum at 514 nm are in line with literature reports.[1] The molecule is insoluble in water;[1] however, when integrated into GUVs fluorescence emission was detected, which was spectrally identical to the fluorescence observed from DCM solutions of the molecule (see Figures 2 and S1); this observation indicates no aggregation of dyes within the lipid bilayer.[42]

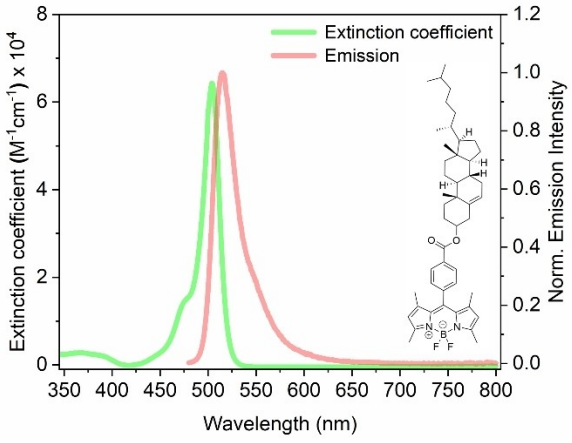

Figure 2. Molecular structure and steady-state spectra of BODIPY-Ar-Chol dissolved in DCM. Green and red colors represent extinction coefficient and emission curve, respectively. For the emission spectrum, the sample was excited at 470 nm.

The unpolarized emission from GUV appears uniform across the bilayer ring (Figure S1). However, when the GUV is excited with polarized light and the emission is recorded under defined polarization angles, only the BODIPY molecules with transition dipole moment aligned along the excitation polarization (bidirectional arrows in Figure 3a and 3b) get excited due to photoselection.[43] For excitation polarized along the x-direction, high emission is observed from locations 1 and 3 (Figure 3a) of the GUV. This indicates that the molecules at these locations have a preferred orientation of the dipole moment along the x-direction. Similarly, for the excitation polarized along the y-direction (Figure 3b), high emission is observed from locations 2 and 4 due to molecules having the dipole moment oriented along the y-direction on two sides. In the molecular frame, the transition dipole moment of the BODIPY chromophore is oriented along the long axis of the BODIPY-core.[43–45] The observed photoselection clearly indicates highly ordered BODIPY molecules, that are aligned along the lipid bilayer membrane plane. The anisotropy, which is obtained from the difference between two orthogonal fluorescence intensities (see SI Equation S2), appears high (r~0.4) where emission with a particular polarization is high and emission along the orthogonal direction is lower by a factor of two. For excitation polarization along the x-direction (Figure 3c), fluorescence intensity as well as anisotropy at the top and bottom of the GUV, are high; similarly, for the y-directional excitation polarization, high anisotropy is observed on the left-right section of the GUV-embedded BODIPY (Figure 3d). The angle between the dipole moment of the BODIPY chromophore and the normal to the membrane plane is calculated using the fluorescence intensities at the orthogonal positions from Figure 3a. The average of 40 pixels from two orthogonal positions (near 1 & 2 or 3 &4) are

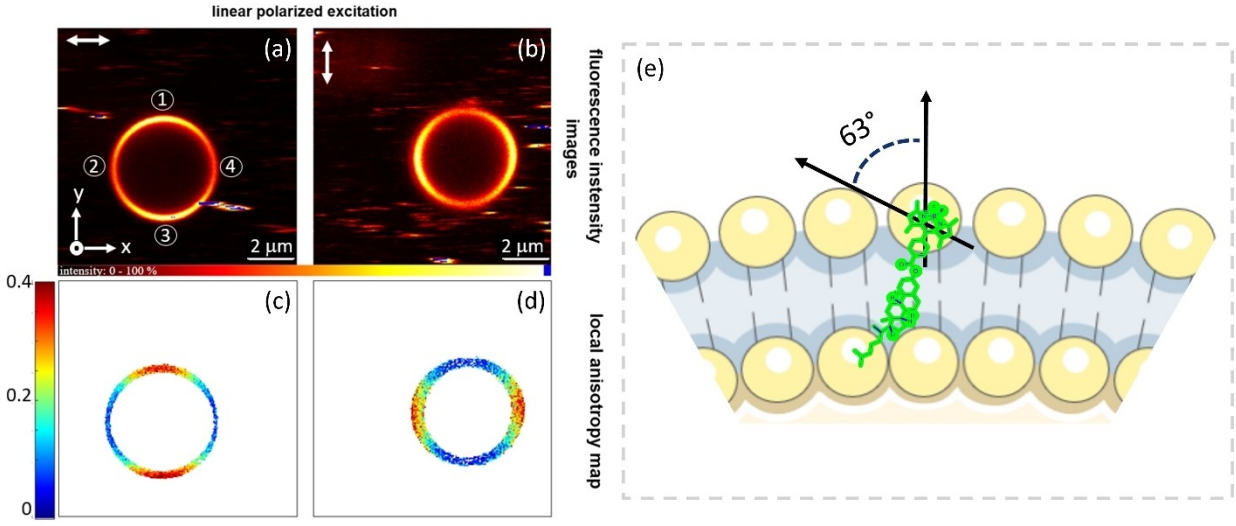

Figure 3. Confocal fluorescence images at the equatorial plane of a DOPC GUV with BODIPY-Ar-Chol reconstituted into the lipid bilayer. (a,b) Normalized fluorescence intensity images for two orthogonal linearly polarized excitations (excitation polarization indicated by the arrows, detected as parallel-polarized emission, $I_{\parallel}$). The 1–4 numbers in the image denote different locations in the equatorial plane of the GUV. (c,d) Anisotropy maps of BODIPY-Ar-Chol in the lipid membrane for the two linearly polarized excitations shown in (a) and (b), respectively. Color-coding for anisotropy values is shown according to the color bar. Intensity thresholds were set to exclude the non-membrane areas of the images. (e) Schematic representation of the BODIPY molecule in the lipid bilayer. The arrow along the long axis of BODIPY represents the mean transition dipole moment and the vertical arrow represents the normal axis to the lipid membrane surface. The schematic does not represent the size of lipids and BODIPY-Ar-Chol molecule.

used in Equation S8 which reveals that the angle between the transition dipole moment and the normal to bilayer membrane is $63 \pm 2°$. Due to averaging over many pixels, the angle obtained is an average angle of all BODIPY molecules in these pixels. A similar scenario has been suggested by Karolin et al.;[46] they embedded BODIPY-derivatives in lipid bilayers of DOPC and observed the transition dipole moment of the BODIPY perpendicular to the normal to bilayer plane. However, these authors used fluorescence anisotropy of GUVs and arrived at their structural proposition based on the (slow) fluorescence anisotropy measurements, the consideration of an order parameter and linear dichroism measurements.[46] When the angle between the transition dipole moment of the molecule and normal to membrane plane is more than the magic angle (54.7°), distinct high and low fluorescence intensities (as well as anisotropies) have been observed for Nile Blue[47] and several other molecules[43,48,49] in orthogonal sections of the lipid bilayer.

Having established detailed insight into the orientation of the BODIPY-fluorophore in the lipid bilayer membrane, its rotational dynamics upon excitation were then investigated. In a BODIPY-phenyl FMR, two distinct molecular rotations can take place. First, intramolecular rotation (segmental mobility), during which the phenyl ring which has a smaller moment of inertia, rotates faster with respect to BODIPY moiety which has a larger moment of inertia.[3] For the molecule investigated here, although the presence of methyl groups at positions 1,7 restricts the free rotation of the phenyl group, there is still motion (though somewhat restricted) between the BODIPY and phenyl group possible. Literature reports that the addition of substituents on the ortho and meso position of the phenyl ring enhances the emission quantum yield due to further restriction of rotation of the phenyl ring.[2,50–52] Hence, there is finite segmental mobility between the BODIPY and the phenyl ring. TDDFT calculations predict a BODIPY-phenyl rotation of about 24° going from the Frank-Condon region (S_0 geometry) toward the geometry of the emissive state (S_1), see SI Table S3. Second, the BODIPY-phenyl FMR can rotate as a single entity; a motion in the excited state that finally equilibrates the distribution of dipole moment. Due to the comparably large moment of inertia of the BODIPY-moiety, this rotation is significantly slower than the intramolecular rotation.[53,54] Consequently, in low-viscosity solvents, the intramolecular rotation dominates the emission decay properties. However, in highly viscous media the intramolecular rotation is slowed due to the high-volume demand of the motion, which enhances the emission intensity and increases the lifetime; as well as the overall rotation of the FMR as a single entity is slowed.[3,55,56]

Time-resolved emission anisotropy (TEA) and transient absorption anisotropy (TAA) are performed to obtain the rotational dynamics of the molecule. The transient emission (recorded at 514 nm), transient absorption (recorded at 525 nm) magic angle kinetics and anisotropy of the BODIPY-Ar-chol in DCM and GUV are shown in Figure S4 and Figure 4, respectively. See SI equations S1 and S2 for the calculation of magic angle signal and anisotropy.

The magic angle kinetics (Figure S4) show negative ΔAbs signals at around 525 nm indicating contributions from ground-state bleach (GSB) and stimulated emission (SE), which is consistent with the steady-state spectra (Figure 2) and literature reports on BODIPY-derivatives.[53,57] The anisotropy data presented in Figures 4 fall in the range between $r(t) = 0.4$ to 0.04, with a few data points larger than $r(t) = 0.4$ for GUV samples (Figure 4d). These data points are considered outliers due to the larger margin of error (±20% of the measured ΔAbs). Generally, different anisotropies recorded at long delay times (*ca.* 2 ns) can be observed when comparing BODIPY-Ar-chol in solution to the BODIPY dyes anchored to GUVs: In the DCM solution, the initial anisotropy of about 0.4 drops to ca. 0.04 at 2 ns, while the long-delay time anisotropy for the molecule anchored to GUVs is *ca.* 0.1 in 2 ns. High initial anisotropy reveals that absorption and emission transition dipoles are collinear.[47,58,59] The TDDFT calculations also show a marginal 0.13° angle between the two transition dipoles (see, SI Table S2).

The anisotropy decay components of a molecule depend upon its shape. A rigid spherical molecule has only one anisotropy decay and corresponding rotational relaxation time.[58] However, when a molecule is non-spherical, it can be modelled as an ellipsoid. The anisotropy decay of such a molecule is the sum of exponential terms based on the rotational diffusion coefficients of its different axes.[58,60,61] The non-spherical structure of BODIPY-Ar-Chol can be approximated by an ellipsoid with three axes with dimensions of 21.6 Å, 6.1 Å and 4.5 Å along the x, y and z axes, respectively, as shown in Figure 5a. In the molecular frame shown in Figure 5a, the absorption and emission transition dipoles are along the y-axis, *i.e.*, perpendicular to the long axis (x-axis). Rotation around the long axis (x-axis) is supposed to be faster because of less displacement of solvent molecules around this axis; conversely, rotation around the short axis (y axis) is supposed to be slower because of the large displacement of solvent molecules.[58]

The TAA in DCM decays with three characteristic time constants 2 ps, 43 ps and 440 ps (see Figure 4b). The two time-constants may arise from the rotational diffusion around the three axes, as shown in Figure 5. Ariola et al. obtained two time-constants 180 ps and 800 ps for a structurally similar BODIPY-col molecule from time-resolved emission anisotropy decay in dimethyl sulfoxide ($\eta_{DMSO} = 2$ cP, at 293 K);[17] Because the viscosity of DCM ($\eta_{DCM} = 0.43$ cP, at 293 K)[62] is ~5 times lower than the viscosity of DMSO, faster rotational relaxation time of 550 ps is obtained for the BODIPY-Ar-Chol molecule in DCM by TEA (Figure 4a) in this work. The better resolution of the TAA employed in this work enables us to resolve all three rotational relaxation times. Similar to the TEA anisotropy decay recorded here, for several other BODIPY-derivatives only one rotational relaxation time could be resolved using TEA.[53,54,63]

Previously, it has been reported that segmental motion (intramolecular rotation) of the chromophore can also change the orientation of the transition dipole moment; hence, contributing to decay of the anisotropy.[58,64] We investigated the effect of segmental mobility on the orientation of the transition dipole moment within the molecular frame using

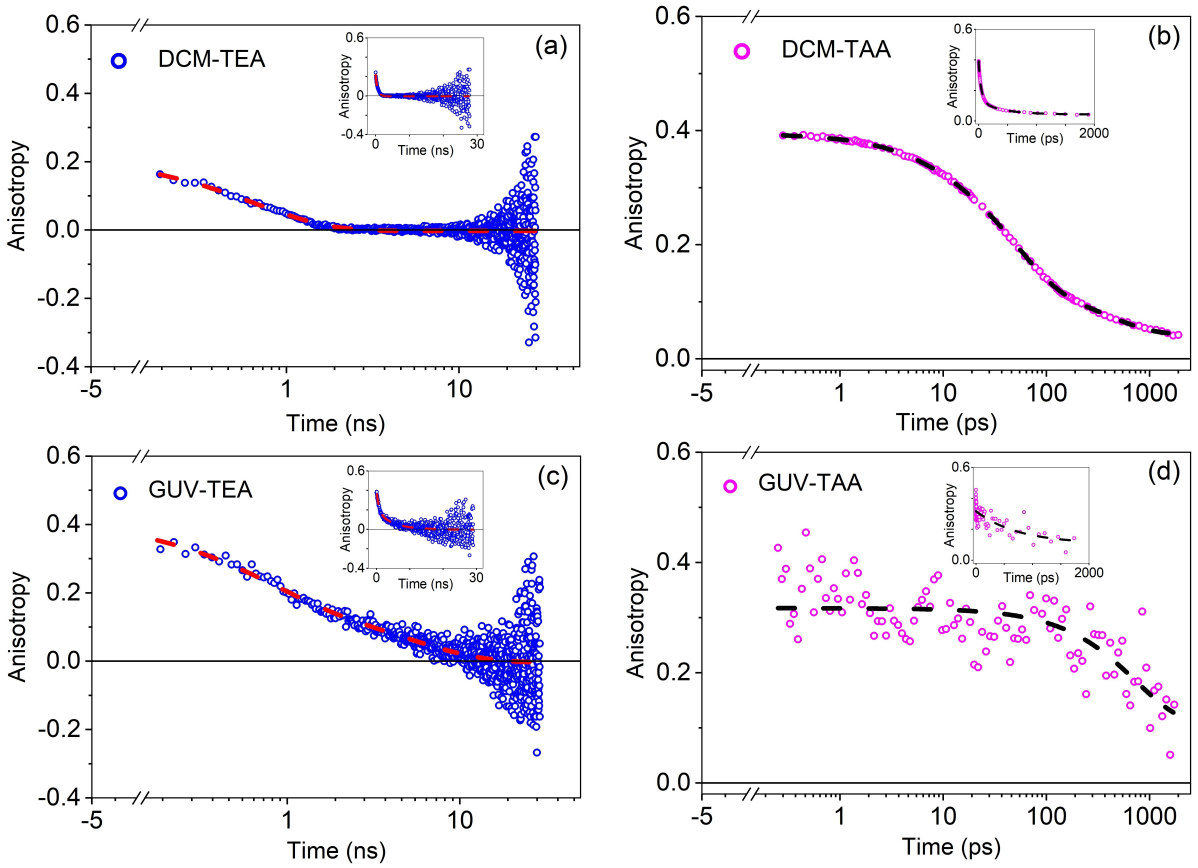

Figure 4. BODIPY-Ar-Chol anisotropy. (a) TEA in DCM, mono-exponential fit in red yields a lifetime of 550 ps with an error value within 20% of the given value, χ^2 (reduced) ≈0.03. (b) TAA in DCM, triexponential fit in red yield lifetimes of 2 ps, 43 ps and 440 ps; the error value is within 5% of the given value, χ^2 (reduced) ≈10^{-5}. (c) TEA in GUV, biexponential fit in red yields lifetimes of 700 ps and 5.1 ns, with an error value within 20% of the given values, χ^2 (reduced) ≈0.04. (d) TAA in GUV, mono-exponential fit in black yields a lifetime of 700 ps, with an error value within 20% of the given value, χ^2 (reduced) ≈0.02.

TDDFT calculations. The geometrical relaxation from the S_0 state to the S_1 state leads to a change of orientation of less than 1° (see SI, Table S4). Furthermore, by investigating the potential energy surface along the BODIPY-phenyl dihedral angle, we could estimate that the transition dipole moment direction changes by about 3° for thermally accessible rotations (see SI, Table S6).

Similarly, solvation-induced temporal changes in anisotropy have also been reported for solute-solvent pairs.[25,65] We investigated the solvation induced anisotropy decay using TDDFT calculations performed with a polarizable continuum model (Tables S7–S8), it predicts a small rotation (~0.3°) of the transition dipole moment in the molecular frame due to solvent relaxation.

We provide two possible origins for the fastest anisotropy decay (2-ps) component. First, it may be attributed to intramolecular structural relaxation. In particular, previous studies associated rotation of the BODIPY chromophore with respect to an organic chromophore attached, instead of the phenyl used in the molecular structure here, to a sub-5 ps process.[53,65,66] Thus, such very fast intramolecular rotation accounts for about 7% of the anisotropy decay (see SI, Table S1).[58] Second, rotational motion around the z-axis contributes to the fast, sub-5 ps process. Such motion is calculated to move solvent in a volume of 1838 Å^3, compared to volumes of 11984 Å^3 and 3402 Å^3 associated with rotations along the y- and x-axis, respectively (see, computation section for details); likely, the corresponding rotational relaxation times 440 ps and 43 ps may arise from rotations along the y- and x-axis, respectively. Small and Isenberg indicated, in seminal work, that small changes in the molecular axis length can cause significant changes in the rotational diffusion timescales.[60] Following this argument, the fastest anisotropy decay component may have contributions from molecular rotation around the z-axis.

When reconstituted into a GUV comprised of DOPC, the motion of the BODIPY-conjugate becomes hindered, i.e., the chromophore probed in transient absorption anisotropy experienced an increased local viscosity.[3,17,18,67] This was reflected in the experimental transient-absorption anisotropy (Figure 4d), which revealed a 700 ps characteristic time constant for the decay. However, the anisotropy did not decay to zero within 2 ns. We note that the TAA measurement could not be extended beyond 2 ns due to the limitation of the optical delay line. The TEA measurement which is not limited to this constraint recorded the anisotropy decay up to 25 ns (Figure 4c) and revealed two time-constants of 700 ps and of 5.1 ns. Both time-constants in lipid bilayer medium are slower than the time-constants observed in DCM, which is associated with the

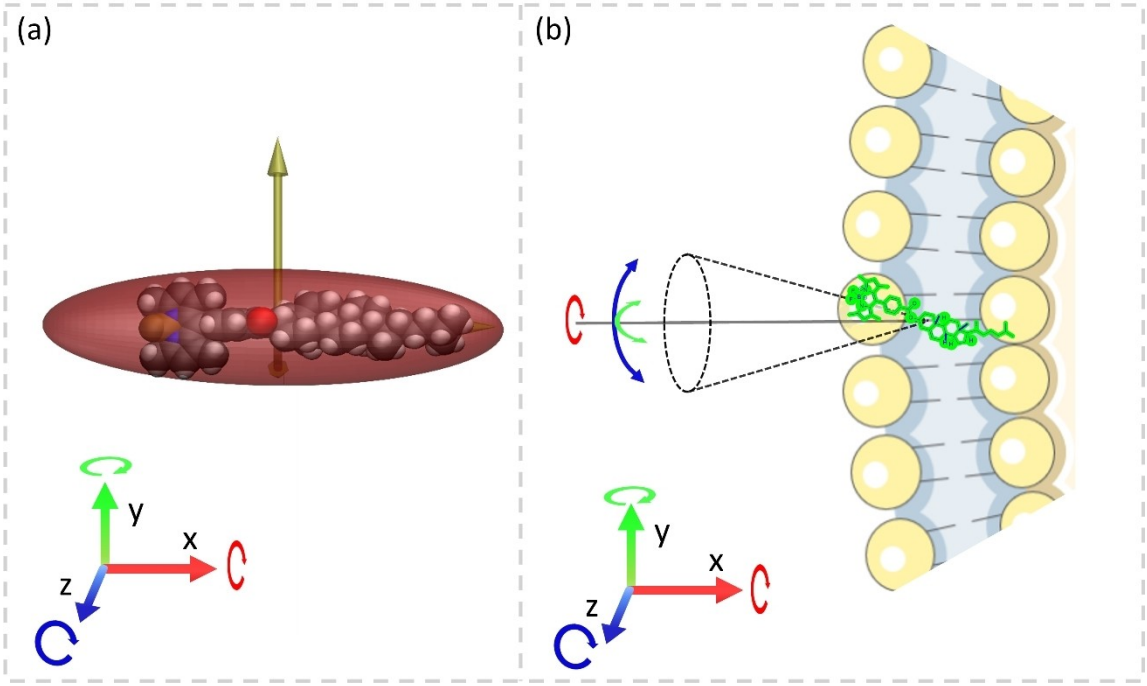

Figure 5. (a) The Van-der-Waals surface of the BODIPY-Ar-Chol molecule with the principal axes depicted as arrows and the Löwner-John ellipsoid associated with it. The three axes of the ellipsoid are shown along x (red), y (green) and z (blue) axes. The circular arrow represents the rotational diffusion around each axis. (b) The wobble-in-cone motion of the BODIPY-Ar-chol molecule in the lipid bilayer: The fast rotation (700 ps) around the x axis and slow wobble motion (5.1 ns) around the y and z axes.

steric constraints of the high viscosity of the lipid bilayer (*vide infra*). The two time-constants are most likely related to the wobble-in-cone motion of the BODIPY-Ar-chol molecule in high viscosity lipid bilayer media.[68–70] The molecule is rigidly embedded in the membrane, its BODIPY-moiety is near the polar headgroups and the cholesterol is placed parallel to the acyl-chain of the DOPC (*vide supra*);[17,18,46,71] the slow time-constant 5.1 ns may arise from the slow back-and-forth flip (wobble) motion away from the normal and 700 ps may arise from the rotation around the long axis of the molecule, as shown in the Figure 5b.

The average rotational relaxation time-constants are 142 ps and 2.1 ns in DCM and in DOPC GUV, respectively, as calculated using Equation S5, see SI Table S1 for details. We estimated a microviscosity of 6.4 ± 1.2 cP in the GUV using Equation S6, which is in line with the previous reports on the microviscosity of homogeneous GUVs made of DOPC.[67]

To summarize, the TAA is advantageous in obtaining the anisotropy of non-spherical molecules as well as fast anisotropy decay down to the sub-picosecond timescale, which is beyond the resolution limit of most of the time-resolved fluorescence emission measurement systems. Such temporal resolution is essential in understanding the anisotropy decay components due to fast rotation along long axis of the molecule.[58,64,65] The slower decay components obtained using TEA are essential to investigate the rotational relaxation motion in high viscous media.[13,46,72] Therefore, the methods are highly complementary and combined can give complete insight into the motion of a probe and microviscosity of its environment.

The methodology can be used further to investigate the microviscosity of ternary GUVs with emissive or with non-emissive chromophores as well as in emission-quenched or emission-restricted media since TAA only employs absorption properties of the chromophore. Our study can further be translated to the biological cell medium, where physiologically relevant molecules are already studied in cells by (TA) spectroscopy.[24,73] In the context of light-driven drug release using TTAUC, where diffusion of molecules plays a vital role,[5,74] TAA focusing selectively on sensitizer and annihilator molecules in vesicles may contribute to the understanding of the overall upconversion process by providing information on the rotational diffusion times (local diffusion rates, D_R) of the reactants.

Conclusions

Polarization-resolved confocal microscopy, transient absorption anisotropy and transient emission anisotropy of an amphiphilic BODIPY-Ar-Chol molecule embedded into giant unilamellar vesicles (GUVs) were studied. Combined, the methods provide detailed understanding of the fluorophore in solvent and its placement and orientation in a lipid bilayer. The BODIPY-lipids organize themselves in a highly ordered pattern in the lipid bilayer and with an average angle between the transition dipole moment of the fluorophore and normal to the lipid membrane of 63°. The non-spherical shape of the molecule leads to three time-constants of anisotropy decay investigated using transient absorption anisotropy in dichloromethane. The anisotropy

decay components (43 ps, 440 ps) originate from the rotational diffusion around the long (x-axis) and short axis (y-axis) of the BODIPY molecule. In contrast, the anisotropy decay of BODIPY-Ar-Chol in the DOPC lipid bilayer revealed two time-constants associated with wobble-in-cone motion. The transient absorption anisotropy enabled resolution of fast decay components (<50 ps) of the anisotropy whereas the time-resolved emission anisotropy identified a slow decay component (>2 ns) of the anisotropy. Hence, both methods complement each other. The microviscosity of the GUV was calculated using the ratio of average rotational relaxation time-constants in DCM and in a lipid bilayer. Accordingly, the estimated microviscosity of 6.4 ± 1.2 cP was found to be fifteen times the reported viscosity of DCM at 293 K.

Supporting Information

Additional references cited within the Supporting information (Ref. [2, 25, 40, 41, 58, 62, 67, 75–86]).

Acknowledgements

We thank Dr. Mathias Micheel, Dr. Felix Hermann-Westendorf, Dr. Kilian Rolf Anton Schneider and Avinash Chettri for assistance in the initial phase of experiments and Ratnadip De for helpful discussions. KKJ thanks Prof. Ahmed A. Heikal for assistance in hydrodynamic radius calculation. KKJ thanks Dr. Anja Schulz for her academic and nonacademic support. The work was financially supported by the European Commission via grant 813920. MB acknowledges funding by the state of Thuringia and the Deutsche Forschungsgemeinschaft [grant INST 1757/25-1 FUGG] for the Abberior STED microscope. TEK gratefully acknowledges Science Foundation Ireland for funding under grant number [19/FFP/6428]. CE greatly acknowledges financial support by the Deutsche Forschungsgemeinschaft (DFG, German Research Foundation; Germany's Excellence Strategy – EXC 2051 – Project-ID 390713860, and project number 316213987 – SFB 1278) and the State of Thuringia (TMWWDG), and CE is integrated into the Leibniz Center for Photonics in Infection Research (LPI), which is initiated by Leibniz-IPHT, Leibniz-HKI, UKJ and FSU Jena and part of the BMBF national roadmap for research infrastructures. The DFT calculations were performed at the Wrocław Centre for Networking and Supercomputing (grant No. 384) and at the Academic Computer Centre TASK in Gdańsk. Open Access funding enabled and organized by Projekt DEAL.

Conflict of Interests

The authors declare no conflict of interest.

Data Availability Statement

The data that support the findings of this study are available from the corresponding author upon reasonable request.

[1] D. O'Connor, A. Byrne, T. E. Keyes, *RSC Adv.* **2019**, *9*, 22805–22816.
[2] M. K. Kuimova, G. Yahioglu, J. A. Levitt, K. Suhling, *J. Am. Chem. Soc.* **2008**, *130*, 6672–6673.
[3] W. Miao, C. Yu, E. Hao, L. Jiao, *Front. Chem.* **2019**, *7*, 1–6.
[4] M. A. Filatov, *Org. Biomol. Chem.* **2019**, *18*, 10–27.
[5] M. Sittig, B. Schmidt, H. Görls, T. Bocklitz, M. Wächtler, S. Zechel, M. D. Hager, B. Dietzek, *Phys. Chem. Chem. Phys.* **2020**, *22*, 4072–4079.
[6] K. K. Jha, A. Prabhakaran, C. S. Burke, M. Schulze, U. S. Schubert, T. E. Keyes, M. Jäger, B. D. Ivanšić, *J. Phys. Chem. C* **2022**, *126*, 4057–4066.
[7] R. A. Arellano-Reyes, A. Prabhakaran, R. C. E. Sia, J. Guthmuller, K. K. Jha, T. Yang, B. Dietzek-Ivanšić, V. McKee, T. E. Keyes, *Chem. Eur. J.* **2023**, *29*, e202300239.
[8] A. S. Kashirina, I. López-Duarte, M. Kubánková, A. A. Gulin, V. V Dudenkova, S. A. Rodimova, H. G. Torgomyan, E. V Zagaynova, A. V Meleshina, M. K. Kuimova, *Sci. Rep.* **2020**, *10*, 14063.
[9] L. Shimolina, A. Gulin, N. Ignatova, I. Druzhkova, M. Gubina, M. Lukina, L. Snopova, E. Zagaynova, M. K. Kuimova, M. Shirmanova, *Cancers (Basel).* **2021**, *13*, 6165.
[10] E. G. Skurikhin, S. A. Afanas'ev, M. A. Zhukova, T. Yu. Rebrova, E. F. Muslimova, E. S. Pan, N. N. Ermakova, O. V Pershina, A. V Pakhomova, O. D. Putrova, L. A. Sandrikina, L. V Kogai, A. M. Dygai, *Bull. Exp. Biol. Med.* **2021**, *171*, 707–712.
[11] F. Li, S. I. Yang, Y. Ciringh, J. Seth, C. H. Martin, D. L. Singh, D. Kim, R. R. Birge, D. F. Bocian, D. Holten, J. S. Lindsey, *J. Am. Chem. Soc.* **1998**, *120*, 10001–10017.
[12] P. Walde, K. Cosentino, H. Engel, P. Stano, *ChemBioChem* **2010**, *11*, 848–865.
[13] G. F. Schröder, U. Alexiev, H. Grubmüller, *Biophys. J.* **2005**, *89*, 3757–3770.
[14] R. Peters, R. J. Cherrytt, *Proc. Natl. Acad. Sci. USA* **1982**, *79*, 4317–4321.
[15] P. Jain, M. Motosuke, *J. Fluoresc.* **2022**, *32*, 737–743.
[16] L. F. Aguilar, J. A. Pino, M. A. Soto-Arriaza, F. J. Cuevas, S. Sánchez, C. P. Sotomayor, *PLoS One* **2012**, *7*, e40254.
[17] F. S. Ariola, Z. Li, C. Cornejo, R. Bittman, A. A. Heikal, *Biophys. J.* **2009**, *96*, 2696–2708.
[18] L. M. Solanko, A. Honigmann, H. S. Midtiby, F. W. Lund, J. R. Brewer, V. Dekaris, R. Bittman, C. Eggeling, D. Wüstner, *Biophys. J.* **2013**, *105*, 2082–2092.
[19] T. A. Smith, K. P. Ghiggino, *Methods Appl. Fluoresc.* **2015**, *3*, 022001.
[20] I. E. Steinmark, P.-H. Chung, R. M. Ziolek, B. Cornell, P. Smith, J. A. Levitt, C. Tregidgo, C. Molteni, G. Yahioglu, C. D. Lorenz, K. Suhling, *Small* **2020**, *16*, 1907139–1907150.
[21] Y. Yuan, B. Liu, *Chem. Sci.* **2017**, *8*, 2537–2546.
[22] Parvathy Venu, Trong-Nghia Le, R. K. Pawan Kumar, Diptendu Patra, C.-K. Lee, R. S. N. Vijayakameswara Rao, *Chem. Asian J.* **2021**, *16*, 2552–2558.
[23] B. L. Youyong Yuan, Chong-Jing Zhang, Meng Gao, Ruoyu Zhang, Ben Zhong Tang, *Angew. Chem. Int. Ed.* **2015**, *54*, 1780–1786.
[24] T. Yang, R. A. Arellano-Reyes, R. C. Curley, K. K. Jha, A. Chettri, Prof. Dr. B. Dietzek-Ivanšić, Prof. Dr. T. E. Keyes, *Chem. Eur. J.* **2023**, *29*, e202300224.
[25] S. Wallin, J. Davidsson, J. Modin, L. Hammarström, *J. Phys. Chem. A* **2005**, *109*, 4697–4704.
[26] C. K. Min, T. Joo, M. C. Yoon, C. M. Kim, Y. N. Hwang, D. Kim, N. Aratani, N. Yoshida, A. Osuka, *J. Chem. Phys.* **2001**, *114*, 6750–6758.
[27] A. Chettri, J. H. Kruse, K. Kumar Jha, L. Dröge, I. Romanenko, C. Neumann, S. Kupfer, A. Turchanin, S. Rau, F. H. Schacher, B. Dietzek, *Chem. Eur. J.* **2021**, *27*, 1–11.
[28] A. J. Wang, K. S. Hu, *Chin. Phys. Lett.* **2002**, *19*, 1727–1729.
[29] R. Siebert, D. Akimov, M. Schmitt, A. Winter, *ChemPhysChem* **2009**, *10*, 910–919.
[30] M. Karnahl, C. Kuhnt, F. Ma, A. Yartsev, M. Schmitt, B. Dietzek, S. Rau, J. Popp, *ChemPhysChem* **2011**, *12*, 2101–2109.
[31] M. J. Frisch, G. W. Trucks, H. B. Schlegel, G. E. Scuseria, M. A. Robb, J. R. Cheeseman, G. Scalmani, V. Barone, G. A. Petersson, H. Nakatsuji, *Gaussian 16, Revision C.01* **2016**.
[32] S. Y. Haoyu, X. He, S. L. Li, D. G. Truhlar, *Chem. Sci.* **2016**, *7*, 5032–5051.
[33] F. Weigend, *Phys. Chem. Chem. Phys.* **2006**, *8*, 1057–1065.

[34] F. Weigend, R. Ahlrichs, *Phys. Chem. Chem. Phys.* **2005**, *7*, 3297–3305.
[35] S. Grimme, *Wiley Interdiscip. Rev.: Comput. Mol. Sci.* **2011**, *1*, 211–228.
[36] S. Grimme, S. Ehrlich, L. Goerigk, *J. Comput. Chem.* **2011**, *32*, 1456–1465.
[37] L. Goerigk, A. Hansen, C. Bauer, S. Ehrlich, A. Najibi, S. Grimme, *Phys. Chem. Chem. Phys.* **2017**, *19*, 32184–32215.
[38] J. Tomasi, B. Mennucci, R. Cammi, *Chem. Rev.* **2005**, *105*, 2999–3094.
[39] A. V Marenich, C. J. Cramer, D. G. Truhlar, *J. Phys. Chem. B* **2009**, *113*, 6378–6396.
[40] R. Schrader, *Oper.-Res.-Spektrum* **1983**, *5*, 1–13.
[41] S. Van Aelst, P. Rousseeuw, *Wiley Interdiscip. Rev. Comput. Stat.* **2009**, *1*, 71–82.
[42] Y. Wu, M. Štefl, A. Olzyńska, M. Hof, G. Yahioglu, P. Yip, D. R. Casey, O. Ces, J. Humpolíčková, M. K. Kuimova, *Phys. Chem. Chem. Phys.* **2013**, *15*, 14986–14993.
[43] S. Brasselet, P. Ferrand, A. Kress, X. Wang, H. Ranchon, A. Gasecka, *Fluorescent Methods to Study Biological Membranes*, (Eds.: Y. Mély, G. Duportail), Springer Berlin Heidelberg **2013**, pp. 311–337.
[44] P. H. Chung, C. Tregidgo, K. Suhling, *Methods Appl. Fluoresc.* **2016**, *4*, e045001.
[45] F. Bergström, I. Mikhalyov, P. Hägglöf, R. Wortmann, T. Ny, L. B. Å. Johansson, *J. Am. Chem. Soc.* **2002**, *124*, 196–204.
[46] J. Karolin, L. B. A. Johansson, L. Strandberg, T. Ny, *J. Am. Chem. Soc.* **1994**, *116*, 7801–7806.
[47] W. Grudzinski, J. Sagan, R. Welc, R. Luchowski, W. I. Gruszecki, *Sci. Rep.* **2016**, *6*, 32780.
[48] Z. Zhou, X. Yan, Y. H. Lai, R. N. Zare, *J. Phys. Chem. Lett.* **2018**, *9*, 2928–2932.
[49] A. Goto, K. Otomo, T. Nemoto, *Front. Phys.* **2019**, *7*, 00056.
[50] A. Loudet, K. Burgess, *Chem. Rev.* **2007**, *107*, 4891–4932.
[51] M. K. Kuimova, *Phys. Chem. Chem. Phys.* **2012**, *14*, 12671–12686.
[52] M. Farfán-Paredes, O. González-Antonio, D. E. Tahuilan-Anguiano, J. Peón, A. Ariza, P. G. Lacroix, R. Santillan, N. Farfán, *New J. Chem.* **2020**, *44*, 19459–19471.
[53] B. Carlotti, M. Poddar, F. Elisei, A. Spalletti, R. Misra, *J. Phys. Chem. C* **2019**, *123*, 24362–24374.
[54] B. Sui, M. V. Bondar, D. Anderson, H. J. Rivera-Jacquez, A. E. Masunov, K. D. Belfield, *J. Phys. Chem. C* **2016**, *120*, 14317–14329.
[55] S. C. Lee, J. Heo, H. C. Woo, J. A. Lee, Y. H. Seo, C. L. Lee, S. Kim, O. P. Kwon, *Chem. Eur. J.* **2018**, *24*, 13706–13718.
[56] B. M. Uzhinov, V. L. Ivanov, M. Y. Melnikov, *Russ. Chem. Rev.* **2011**, *80*, 1179–1190.
[57] S.-Y. Kim, Y.-J. Cho, H.-J. Son, Dae, W. Cho, S. O. Kang, *J. Phys. Chem. A* **2018**, *122*, 3391–3397.
[58] J. R. Lakowicz, *Principles of Fluorescence Spectroscopy*, Springer, Boston, MA, **2006**.
[59] I. D. Johnson, H. C. Kang, R. P. Haugland, *Anal. Biochem.* **1991**, *198*, 228–237.
[60] E. W. Small, I. Isenberg, *Biopolymers* **1977**, *16*, 1907–1928.
[61] S. A. Weinreis, J. P. Ellis, S. Cavagnero, M. M. n, Eunsung Mouradian, *Methods* **2010**, *52*, 57–73.
[62] K. K. Ohligschläger, A. Menzel, K. Ten Kate, A. Martinez, J. R. Frömbgen, C. Arts, J. McCulloch, A. Rossberg, M. Lendle, W. Pfleiderer, G. Tögel, A. Torkelson, T. R. Beutel, *Chloromethanes. In Ullmann's Encyclopedia of Industrial Chemistry* **2022**, *12*, 148–150.
[63] S. D. Usoltsev, O. A. Raitman, A. V. Shokurov, Y. S. Marfin, *J. Mol. Liq.* **2023**, *375*, 121380.
[64] I. Pochorovski, T. Knehans, D. Nettels, A. M. Müller, W. B. Schweizer, A. Caflisch, B. Schuler, F. Diederich, *J. Am. Chem. Soc.* **2014**, *136*, 2441–2449.
[65] E. van Veldhoven, H. Zhang, M. Glasbeek, *J. Phys. Chem. A* **2001**, *105*, 1687–1692.
[66] Y. Dong, M. Taddei, S. Doria, L. Bussotti, J. Zhao, G. Mazzone, M. Di Donato, *J. Phys. Chem. B* **2021**, *125*, 4779–4793.
[67] F. S. Ariola, D. J. Mudaliar, R. P. Walvick, A. A. Heikal, *Phys. Chem. Chem. Phys.* **2006**, *8*, 4517–4529.
[68] K. Kinosita, A. Ikegami, S. Kawato, *Biophys. J.* **1982**, *37*, 461–464.
[69] G. F. Schröder, U. Alexiev, H. Grubmüller, *Biophys. J.* **2005**, *89*, 3757–3770.
[70] T. Fujiwara, K. Nagayama, *J. Chem. Phys.* **1985**, *83*, 3110–3117.
[71] P. Reinholdt, S. Wind, D. Wüstner, J. Kongsted, *J. Phys. Chem. B* **2019**, *123*, 7313–7326.
[72] S. S. Vogel, C. Thaler, P. S. Blank, S. v. Koushik, *Flim Microscopy in Biology and Medicine, Chapman and Hall/CRC* **2009**, 245–288.
[73] K. R. A. Schneider, A. Chettri, H. D. Cole, K. Reglinski, J. Brückmann, J. A. Roque, A. Stumper, D. Nauroozi, S. Schmid, C. B. Lagerholm, S. Rau, P. Bäuerle, C. Eggeling, C. G. Cameron, S. A. McFarland, B. Dietzek, *Chem. Eur. J.* **2020**, *26*, 14844–14851.
[74] T. N. Singh-Rachford, F. N. Castellano, *Coord. Chem. Rev.* **2010**, *254*, 2560–2573.
[75] W. Grudzinski, J. Sagan, R. Welc, R. Luchowski, W. I. Gruszecki, *Sci. Rep.* **2016**, *6*, 1–11.
[76] K. Ball, *Geom. Dedic.* **1992**, *41*, 241–250.
[77] J. Yuan, L. Zhao, G. Leng, *Taiwan. J. Math.* **2007**, *11*, 1315–1325.
[78] F. John, *Comm. Pure Appl. Math.* **1948**, *1*, 149–200.
[79] G. Gervino, G. Mana, C. Palmisano, *Int. J. Mod. Phys. B* **2016**, *30*, 1541002.
[80] P. Bubeck, W. J. W. Botzen, J. C. J. H. Aerts, *Risk Anal.* **2012**, *32*, 1481–1495.
[81] Y. T. Lee, A. Sidford, in *2014 IEEE 55th Annual Symposium on Foundations of Computer Science*, IEEE **2014**, pp. 424–433.
[82] V. M. Tikhomirov, *Am. Math. Mon.* **1996**, *103*, 65–71.
[83] L. A. Nikolov, P. Shushkov, B. Nevado, X. Gan, I. A. Al-Shehbaz, D. Filatov, C. D. Bailey, M. Tsiantis, *New Phytol.* **2019**, *222*, 1638–1651.
[84] Z. Song, X. Yang, Y. Yang, T. Zhou, *arXiv preprint* **2022**, DOI: 10.48550/arXiv.2211.14407.
[85] A. Ben-Tal, A. Nemirovski, *Math. Oper. Res.* **1998**, *23*, 769–805.
[86] M. B. Cohen, B. Cousins, Y. T. Lee, X. Yang, in *Conference on Learning Theory*, PMLR, **2019**, pp. 849–873.

Manuscript received: May 8, 2023
Revised manuscript received: August 30, 2023
Accepted manuscript online: September 9, 2023
Version of record online: September 27, 2023